Patient-Derived Organoids from Multiple Colorectal Cancer Liver Metastases Reveal Moderate Intra-patient Pharmacotranscriptomic Heterogeneity

Bruun, Jarle

2020

Bruun , J , Kryeziu , K , Eide , P W , Moosavi , S , Eilertsen , I A , Langerud , J , Rosok , B , Totland , M , Brunsell , T , Pellinen , T , Saarela , J , Bergsland , C H , Palmer , H G , Brudvik , K , Guren , T , Dienstmann , R , Guren , M G , Nesbakken , A , Bjornbeth , B A , Sveen , A & Lothe , R A 2020 , ' Patient-Derived Organoids from Multiple Colorectal Cancer Liver Metastases Reveal Moderate Intra-patient Pharmacotranscriptomic Heterogeneity ' , Clinical Cancer Research , vol. 26 , no. 15 , pp. 4107-4119 . https://doi.org/10.1158/1078-0432.CCR-19-3637

http://hdl.handle.net/10138/328979
https://doi.org/10.1158/1078-0432.CCR-19-3637

unspecified
publishedVersion

Published OnlineFirst April 16, 2020; DOI: 10.1158/1078-0432.CCR-19-3637

Patient-Derived Organoids from Multiple Colorectal Cancer Liver Metastases Reveal Moderate Intra-patient Pharmacotranscriptomic Heterogeneity

Jarle Bruun[1,2], Kushtrim Kryeziu[1,2], Peter W. Eide[1,2], Seyed H. Moosavi[1,2,3], Ina A. Eilertsen[1,2,3], Jonas Langerud[1,2,3], Bård Røsok[2,4], Max Z. Totland[1,2], Tuva H. Brunsell[1,2,3,5], Teijo Pellinen[6], Jani Saarela[6], Christian H. Bergsland[1,2,3], Hector G. Palmer[7], Kristoffer W. Brudvik[2,4], Tormod Guren[2,8], Rodrigo Dienstmann[7], Marianne G. Guren[2,8], Arild Nesbakken[2,3,5], Bjørn Atle Bjørnbeth[2,4], Anita Sveen[1,2,3], and Ragnhild A. Lothe[1,2,3]

ABSTRACT

Purpose: Molecular tumor heterogeneity may have important implications for the efficacy of targeted therapies in metastatic cancers. Inter-metastatic heterogeneity of sensitivity to anticancer agents has not been well explored in colorectal cancer.

Experimental Design: We established a platform for *ex vivo* pharmacogenomic profiling of patient-derived organoids (PDO) from resected colorectal cancer liver metastases. Drug sensitivity testing ($n = 40$ clinically relevant agents) and gene expression profiling were performed on 39 metastases from 22 patients.

Results: Three drug–response clusters were identified among the colorectal cancer metastases, based primarily on sensitivities to EGFR and/or MDM2 inhibition, and corresponding with *RAS* mutations and TP53 activity. Potentially effective therapies, including off-label use of drugs approved for other cancer types, could be nominated for eighteen patients (82%). Antimetabolites and targeted agents lacking a decisive genomic marker had stronger differential activity than most approved chemotherapies. We found limited intra-patient drug sensitivity heterogeneity between PDOs from multiple (2–5) liver metastases from each of ten patients. This was recapitulated at the gene expression level, with a highly proportional degree of transcriptomic and pharmacological variation. One PDO with a multi-drug resistance profile, including resistance to EGFR inhibition in a *RAS*-mutant background, showed sensitivity to MEK plus mTOR/AKT inhibition, corresponding with low-level *PTEN* expression.

Conclusions: Intra-patient inter-metastatic pharmacological heterogeneity was not pronounced and *ex vivo* drug screening may identify novel treatment options for metastatic colorectal cancer. Variation in drug sensitivities was reflected at the transcriptomic level, suggesting potential to develop gene expression–based predictive signatures to guide experimental therapies.

Introduction

Colorectal cancer accounts for about 10% of all cancer cases and deaths worldwide (1). More than half of all patients with colorectal cancer develop metastatic disease and liver metastasis is the main cause of death (2). Systemic treatment for metastatic colorectal cancer (mCRC) is primarily based on combination chemotherapies with 5-fluorouracil (5-FU), oxaliplatin, and/or irinotecan, with the addition of a few biologically targeted agents such as monoclonal anti-EGFR antibodies in *KRAS*/*NRAS* wild-type (wt) cancers, anti-angiogenic agents targeting VEGF (3, 4), as well as the multi-kinase inhibitor regorafenib (5). These expanded treatment options have improved the median overall survival from approximately one year with 5-FU alone to approximately two–three years with current standard therapies (6). However, almost all patients develop resistance to available therapies (7), and there is an unmet need for more effective therapies and stratified treatment options (8). The potential for this has primarily been documented by the high response rates and durable responses to immune checkpoint inhibitors in the small subgroup of mCRCs with microsatellite instability (9), as well as with targeted combination therapies against $BRAF^{V600E}$ mutations (10) and HER2 overexpression (11).

Patients with mCRC commonly present with multiple metastatic sites, including multiple lesions in the liver. A high level of intra-patient inter-metastatic genomic heterogeneity may be a poor prognostic factor after hepatic resection (12). Clonal expansion is also a major cause of treatment failure, and this has been well documented in mCRC by the emergence of resistant subclones during EGFR inhibition (13). However, it is not well documented to which extent anticancer therapies have the same level of activity in distinct metastatic lesions of each patient, and whether potentially heterogeneous responses may affect patient outcome. Heterogeneous responses both to palliative chemotherapy (14) and to neoadjuvant chemotherapy in

[1]Department of Molecular Oncology, Institute for Cancer Research, the Norwegian Radium Hospital, Oslo University Hospital, Oslo, Norway. [2]K.G. Jebsen Colorectal Cancer Research Centre, Clinic for Cancer Medicine, Oslo University Hospital, Oslo, Norway. [3]Institute for Clinical Medicine, Faculty of Medicine, University of Oslo, Norway. [4]Department of Hepato-Pancreato-Biliary Surgery, Oslo University Hospital, Oslo, Norway. [5]Department of Gastrointestinal Surgery, Ullevål Hospital—Oslo University Hospital, Oslo, Norway. [6]Institute for Molecular Medicine Finland (FIMM), University of Helsinki, Helsinki, Finland. [7]Stem Cells and Cancer Group, Vall d'Hebron University Hospital and Institute of Oncology (VHIO), Barcelona, Spain. CIBERONC, Madrid, Spain. [8]Department of Oncology, Oslo University Hospital, Oslo, Norway.

Note: Supplementary data for this article are available at Clinical Cancer Research Online (http://clincancerres.aacrjournals.org/).

J. Bruun, K. Kryeziu, and P.W. Eide contributed equally to this article.

Corresponding Author: Ragnhild A. Lothe, Oslo University Hospital, Montebello, NO-0424 Oslo, Norway. Phone: 47-2278-1728; Fax: 47-2278-1745; E-mail: Ragnhild.A.Lothe@rr-research.no

Clin Cancer Res 2020;26:4107–19

doi: 10.1158/1078-0432.CCR-19-3637

Published OnlineFirst April 16, 2020; DOI: 10.1158/1078-0432.CCR-19-3637

Translational Relevance

The majority of patient-derived organoids from colorectal liver metastases were sensitive to anticancer drugs in clinical use and/or under development in late-phase clinical trials. Together with only a modest level of intra-patient inter-metastatic pharmacological heterogeneity, this reinforces a potential benefit from off-label use of drugs guided by both pharmacological profiling and established molecular markers. Correlation in the overall variation at the drug sensitivity and gene expression levels supports the relevance of transcriptomic profiling in pharmacogenomic assessments.

patients with resectable colorectal cancer liver metastasis (CRLM; ref. 15) may be associated with a worse survival. Furthermore, there is also evidence of heterogeneous responses to molecularly targeted therapies against HER2 (16) and EGFR, the latter being associated with genomic heterogeneity (17).

The use of genomics to guide cancer therapies has been less successful than anticipated, and less than 7% of patients in 2018 were estimated to benefit from such precision oncology (18). Drug testing of the patient's own tumor cells offers a complementary approach (19). These patient-derived organoids (PDO) recapitulate the genomic and histopathological characteristics of colorectal cancers (20–22). Importantly, several studies have demonstrated that PDOs are amenable to drug screening within a clinically relevant timeframe (20, 23–25), and it was recently shown that PDOs can predict clinical responses (25–27), including to standard combination chemotherapies in a patient with mCRC (28). The pharmacological landscape of PDOs from colorectal cancers has been investigated in a few studies (22, 25, 28), and there is evidence of intra-tumor heterogeneity in responses to selected drugs (29, 30). However, the level of intra-patient inter-metastatic pharmacological heterogeneity is largely unknown. To this end, we have generated a living biobank of PDOs derived from multiple lesions from patients treated for resectable CRLM in an observational study. Our main objective in this pre-clinical phase of the project was to explore intra-patient relative to inter-patient variation in drug sensitivities and gene expression *ex vivo*.

Materials and Methods

Patients and tissue sampling

Twenty-nine patients treated for resectable CRLM within fifteen months of an ongoing observational study at Oslo University Hospital, from September 2017 to November 2018, were included. All patients, except for patient 28, had received standard combination chemotherapies with or without targeted agents before the liver resection from which the studied tumors were sampled and PDOs were derived, either as a part of a prior treatment regimen ($n = 6$) or as neoadjuvant treatment ($n = 15$; Supplementary Table S1). Parallel tissue samples were immediately frozen (−80°C) for molecular profiling or submitted to organoid cell culture within 1 to 18 hours. Samples for PDO cell culture were transported on ice in basal culture media (Advanced DMEM/F-12 #12634028 supplemented with 10 mmol/L HEPES #15630080, 2 mmol/L GlutaMAX #35050061, and 100 U/mL penicillin-streptomycin #15140122, all from Thermo Fisher Scientific/Gibco).

The study was approved by the Norwegian Data Protection Authority and the Regional Committee for Medical and Health Research Ethics, SouthEastern Norway (2010/1805; 2017/780). Written informed consent was obtained from all patients included in the study. The research performed was consistent with the Declaration of Helsinki, and the research biobanks were constructed in compliance with national legislation.

Organoid cell culture

Organoid cell culture was based on the methods described by Fujii and colleagues (refs. 22, 31; Supplementary Methods). All PDO cultures were periodically tested for *Mycoplasma* contamination using the MycoAlert Mycoplasma Detection Assay (Lonza #LT07-518) and their identities verified by short tandem repeat profiling according to the AmpFℓSTR Identifiler PCR Amplification Kit (Thermo Fisher Scientific). One PDO culture did not match the patient's original tumor profile and was discarded from further analyses.

Drug library and sensitivity screening

A customized drug library was designed for drug response profiling of the PDOs, including a total of 40 anticancer agents either used as standard of care to treat colorectal cancer, drugs approved for other indications, drugs under development (in clinical trials for colorectal cancer), or agents identified from high-throughput drug screening of colorectal cancer cell lines (ref. 32; Supplementary Table S2). Drugs (at nine concentrations typically ranging from 1 to 10,000 nmol/L) and controls (100 μmol/L benzethonium chloride in nine wells as positive control and 0.1% DMSO in 13 wells as negative control) were preprinted onto 384-well tissue culture plates (Corning 3707 clear black flat-bottom microplates) using liquid acoustic dispensing technology (Echo 550, Labcyte Inc.; printed at the High Throughput Biomedicine Unit at the Institute for Molecular Medicine Finland), except for the monoclonal antibody cetuximab which was added manually at two concentrations (5 and 50 μg/mL) immediately before screening. Two replicate 384-well plates were screened per sample. Using an Integra Voyager electronic multichannel pipette, 10 μL of Matrigel was added to the bottom of each well before seeding 450–600 organoids (strained with a 40-μm pore size mesh from VWR, #734-0002) to a final volume of 40 μL in 3% Matrigel/ENAS media supplemented with 10 μmol/L ROCKi, and incubated at 37°C in a humidified 5% CO_2 atmosphere. Viability was measured after 96 hours of drug exposure using the CellTiter-Glo 3D Cell Viability Assay (Promega) according to the manufacturer's instructions and measured on a Victor 3 microplate reader (PerkinElmer).

CellTiter-Glo luminescence (*lum*) readouts were rescaled to relative viability ($\tilde{E}$, measured viability) based on the median of the control wells with 0.1% DMSO as negative control (NC, viability = 1) and 100 μmol/L benzethonium chloride as positive control (PC, viability = 0). Thus for drug j at concentration x, viability was defined as follows

$$\tilde{E}_{j,x} = 1 - \frac{lum_{NC} - lum_{j,x}}{lum_{NC} - lum_{PC}}$$

Technical replicates were rescaled separately and data combined to estimate dose–response curves. $\tilde{E}_j$ was truncated to lie between 0 and 1 and we fitted logistical models using the function logLogisticRegression in the R package PharmacoGx (v1.14.2; ref. 33).

$$E(x; slope, E_\infty, EC_{50}) = E_\infty + \frac{1 - E_\infty}{1 + \frac{x}{EC_{50}}^{slope}}$$

Here, E refers to the modeled viability and x refers to the drug concentration [all values in nanomolar (nmol/L) if not otherwise specified]; *slope* refers to the Hill coefficient (steepness) of the curve; E_∞ refers to the asymptote as x tends to infinity; and EC_{50} refers to the concentration at half maximum effect [i.e., $E(EC_{50}) = \frac{1}{2}(1 + E_\infty)$].

Published OnlineFirst April 16, 2020; DOI: 10.1158/1078-0432.CCR-19-3637

E_{max} is defined as the modeled viability at the maximum assayed drug concentration. Drug sensitivity scores (DSS) were calculated using the function DSS in the R package DSS (v1.2) with the following parameterization: $IC_{50} = EC_{50}$; SLOPE = *slope*; MIN = 0; MAX = $(1-E_{\infty}) \times 100$; $y = 10$; type = 2 (34). All dose–response models [n = (40 drugs + 1 combination) × 39 samples = 1,599] were visually assessed and for problematic fits manually set to either the result from the higher-quality replicate ($n = 2$) or NA if ambiguous ($n = 32$). For disulfiram+Cu, five concentrations were excluded due to printing errors whereas for olaparib and erastin the highest concentration was excluded due to noise, possibly due to precipitation, and dose–response models were refitted. For SN-38, four concentrations were discarded due to loss of activity on one of two source plates (dose–response curves were fitted on the basis of concentrations 1, 3, 100, 300, and 10,000 nmol/L). 2-methoxyestradiol and sirolimus were discarded due to batch effects (loss of activity).

The quality of each drug screen plate was evaluated on the basis of the strictly standardized mean difference (SSMD) metric and a single sample (two technical replicates) with SSMD < 3 was discarded and repeated. For the remaining screens the median SSMD was 9.25 (range, 3.03–34.3). Drug variability was evaluated on the basis of the standard deviation (SD) of the differences in DSS for technical replicates (Supplementary Fig. S4C). Drugs with SD > 3.1 ($n = 3$) were excluded from principal component analyses. For the remaining drugs, the median SD was 1.41 (range, 0.16–3.01).

Drug synergy screening

On the basis of the single-agent results, a customized combination screen was designed for drug synergy profiling of one PDO. Drug combinations were printed on a 384-well plate with each assay covering 48 wells and forming a (7 × 7)−1 dose–response matrix. As for the initial screen, relative cell viabilities were assessed using the CellTiter-Glo 3D Cell Viability Assay (Promega) following 96-hour incubation. The highest concentration combinations were imputed with the maximum for a full 7 × 7 matrix. Following normalization, the resulting data were used as input for the SynergyFinder web application https://synergyfinder.fimm.fi (accessed 2019 June 12) and drug interaction landscape probed using a zero interaction potency (ZIP) model that captures the drug interaction relationships by comparing the change in the potency of the dose–response curves between individual drugs and their combinations (35).

Gene expression analyses

Gene expression profiles were generated for the 39 PDOs that were successfully screened for drug sensitivities using the GeneChip Human Transcriptome Array 2.0 according to the manufacturer's instructions (Thermo Fisher Scientific). Parallel tissue samples for a subset of 18 of the metastases were also analyzed, including two tissue samples from each of 3 metastases (total of 21 samples). Raw intensity data stored in CEL files were background corrected, quantile normalized, and summarized at the gene level according to the robust multi-array average (RMA) approach with R package affy (v1.62.0) and independently with modified Signal Space Transformation implemented in the Affymetrix Expression Console 1.1 software. For comparison, the gene expression datasets for PDOs and tumor tissue samples were merged by batch correction using ComBat (36) implemented in the R package SVA (37). Before pair-wise correlation analyses between samples, the expression level of each gene was centered and scaled using the mean expression level and standard deviation among all samples, respectively. For the tumor tissue samples, a liver enrichment score was calculated on the basis of a set of genes ($n = 157$) with expression enrichment in the liver (downloaded from The Human Protein Atlas; https://www.proteinatlas.org/humanproteome/tissue/liver) using the R package GSVA (38).

A gene expression signature for *TP53* mutations was generated by differential expression analyses between mutated and wild-type tumors in our previously published gene expression dataset of 409 primary colorectal cancers (GEO accession numbers GSE24550, GSE29638, GSE69182, GSE79959, GSE97023, and GSE96528) using the R package limma. Sample-wise gene set enrichment scores for TP53wt signature were calculated using the "gsva" function in the R package GSVA based on the 5 most differentially expressed genes ranked by *P* value (all downregulated in *TP53* mutated tumors; *MDM2, SPATA18, FAS, DDB2, HSPA4L*). The same function was used to calculate single-sample enrichment scores for 14 gene sets assembled from different databases (39). EGFRi- and MEKi-responder signatures were retrieved from ref. 23 (16 genes) and ref. 40 (66 genes), respectively.

DNA/RNA isolation and gene mutation analyses are described in Supplementary Methods and Supplementary Table S1.

Immunostaining

All PDOs were paraffin embedded and stained for hematoxylin and eosin, as well as the epithelial colorectal cancer markers caudal type homeobox 2 transcription factor (CDX2), cytokeratin 7 (CK7), and cytokeratin 20 (CK20; details in Supplementary Methods).

Statistical analyses

All statistical analyses were performed in R (version 3.6.2), including unsupervised principal component analyses of gene expression data [based on the genes ($n = 2{,}000$) with highest cross-sample variance] using the package FactoMineR or stats, correlation analyses using the function "cor," linear models using the function "lm," and two-samples *t* test using the function "t.test" and Wilcoxon rank sum test using the function "wilcox.test".

Binomial confidence intervals were calculated using the function "binconf" in the R package Hmisc (v4.2-0). Heatmaps were prepared using the R package heatmap3 with clustering and agglomeration as indicated in captions. To account for multiple drugs with a similar mechanism of action (e.g., afatinib/cetuximab/erlotinib/lapatinib and binimetinib/trametinib) in the overall sensitivity analysis, the function "findCorrelation" in the R package caret (v6.0-84) was used to filter drugs with absolute pair-wise correlation above 0.75 ($n = 3$).

Results

Drug sensitivity and gene expression profiling of PDOs from resected CRLMs

An overview of the *ex vivo* pharmacogenomic platform for analysis of PDOs derived from resected CRLMs is shown in **Fig. 1A**. Tumor cells were isolated from multiple CRLMs ($n = 75$ lesions) from twenty-nine patients and cultured *ex vivo*. PDOs were successfully established for 39 lesions (lesion-wise success rate 52%) from twenty-two patients [patient-wise success rate 76%; 95% binomial proportion confidence interval (CI): 58%–88%; Supplementary Table S1], including five distinct metastatic lesions from one patient, three lesions from four patients, two lesions from another five patients, and one lesion from twelve patients (**Fig. 1B**). There was a moderate correlation between the number of lesions attempted to culture per patient and the numbers of successfully established PDOs ($r = 0.39$, $P = 0.035$, Pearson's correlation test, **Fig. 1B**), indicating that successful culture was not only dependent on the number of sampled tumors per patient, but also on the biological traits of the sampled cancer cells. Most PDOs

Published OnlineFirst April 16, 2020; DOI: 10.1158/1078-0432.CCR-19-3637

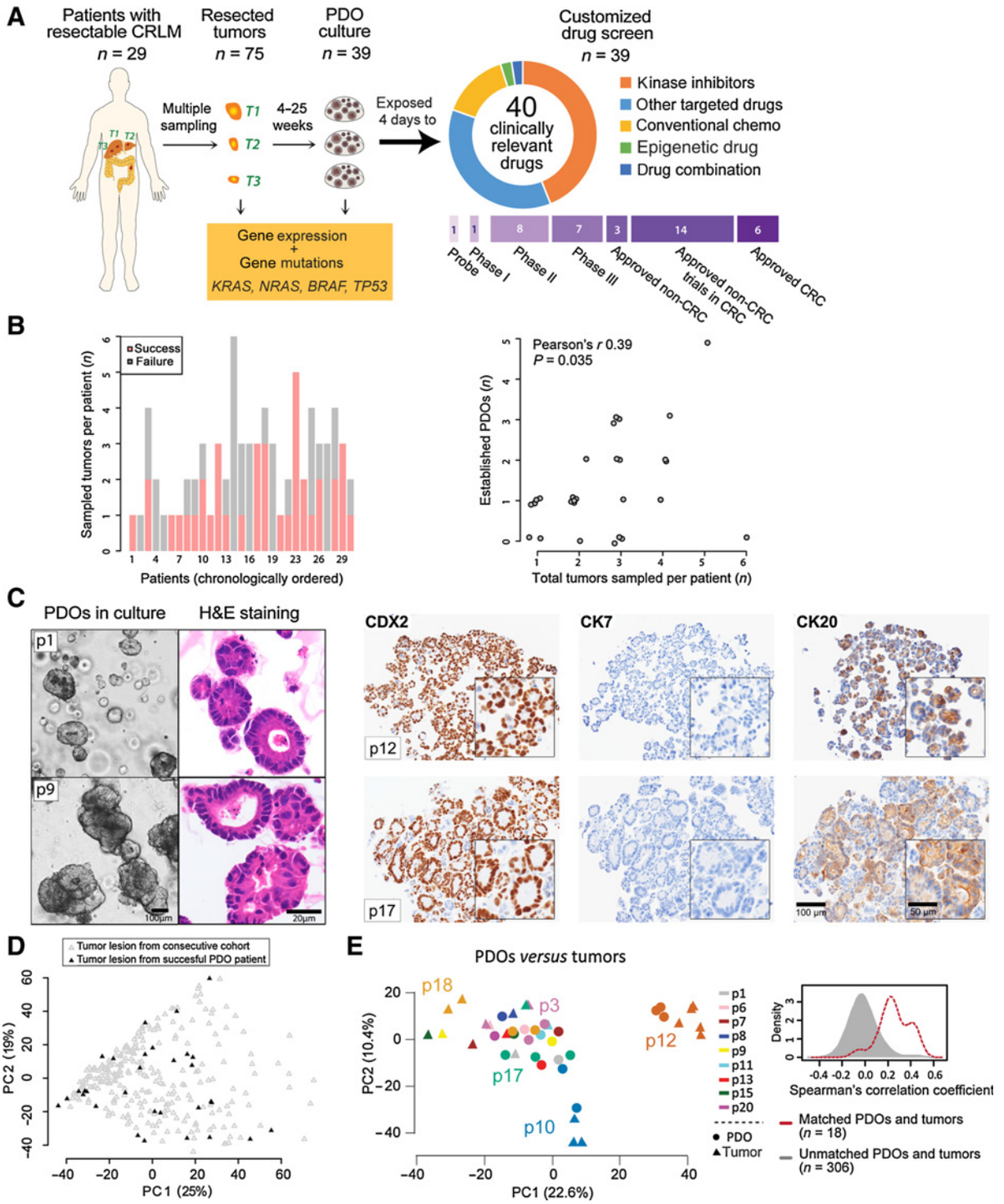

Figure 1.

A living biobank of colorectal cancer liver metastases (CRLM). **A,** Included patients and study overview. **B,** PDO growth success rate and the number of lesions. **C,** PDO growth morphologies and epithelial markers. CDX2, caudal type homeobox 2 transcription factor; CK7, cytokeratin 7; CK20, cytokeratin 20. **D,** Representativeness of the PDO cohort. Unsupervised principal component analysis of gene expression data highlighting lesions from patients with successful PDO cultures (black, $n = 31$ tumors from 14 patients) in the context of the in-house consecutive cohort of surgically treated patients with colorectal liver metastases ($n = 290$ tumors and $n = 174$ patients). **E,** Principal component analysis plot showing correspondence between gene expression from individual PDOs and their respective tumors. Multiple-lesion CRLMs and corresponding PDOs from five patients are indicated with colors and numbers inside the plot, whereas single-lesion CRLMs and corresponding PDOs are shown in the legend. Distributions of Spearman's correlation coefficients are from matched and non-matched PDOs and tumors. For twenty-one PDOs analyzed, corresponding tumor tissue was not analyzed. p, patient; PC, principal component.

Published OnlineFirst April 16, 2020; DOI: 10.1158/1078-0432.CCR-19-3637

had an epithelial architecture and presented with a lumen enclosed by a single epithelial cell layer (**Fig. 1C** left and Supplementary Fig. S1). Epithelial colorectal cancer tissue origin was assessed by immunostaining of the proteins CDX2, CK7, and CK20 (**Fig. 1C** right and Supplementary Fig. S2). The PDOs exhibited large differences in growth rates and the time from tumor resection to completed drug screening varied from 3.7 to 25 weeks (median = 9.2 weeks).

Representativeness of the PDOs for the resected CRLMs was evaluated by gene expression profiling. Principal component analysis (PCA) of a subset of the corresponding tissue samples showed that the tumors grown as PDOs were representative of a large in-house consecutive cohort of resected CRLMs ($n = 290$ tumors; 174 patients, 1–15 tumors per patient, unpublished data; **Fig. 1D**). Furthermore, gene expression profiles of these PDOs and their original tumors showed an overall fair clustering (**Fig. 1E**). The mean Spearman's correlation coefficient between matched PDOs and tumors was significantly higher than the mean between unmatched PDOs and tumors (difference in mean Spearman's correlation = 0.27, $P = 1.3 \times 10^{-9}$). Principal component (PC) 2 of the tumor samples (but not PC1) correlated with a gene expression–based enrichment score for liver-specific genes (Supplementary Fig. S3), showing that infiltration of non-malignant cells in the tumor microenvironment has an important impact on gene expression signals in the tissue samples, and this is a likely explanation for deviations between some of the tumors and the corresponding PDO.

All PDOs were evaluated for sensitivities to thirty-eight clinically relevant drugs (Supplementary Table S2) and sensitivities were calculated as DSS values (34), representing the area over the dose–response curve across nine different concentrations of each drug. Replicate screens for each PDO showed a high technical reproducibility, with a median Pearson's correlation coefficient across samples of 0.98 (range 0.87–0.99, Supplementary Fig. S4A and S4B). Notably, the reproducibility varied among the different drugs and two drugs (ipatasertib and linsitinib) had a particularly high variability between technical replicates (SD = 5.5 and 6.4, respectively; Supplementary Fig. S4C). Replicate screens of ten PDOs performed from 1 to 17 months apart and following a freeze/thaw cycle showed strong biological reproducibility, with Pearson's correlations ranging from 0.81 to 0.93 (Supplementary Fig. S4D). Also, drugs with a similar mechanism of action clustered together in hierarchical clustering based on Pearson's correlations (Supplementary Fig. S5). Comparisons of the three drugs targeting EGFR (afatinib, cetuximab, and erlotinib) showed Pearson's correlation coefficients ranging from 0.86 to 0.94, and the two drugs targeting MEK (binimetinib and trametinib) had a correlation of 0.80. Resistance to EGFR inhibition was confirmed in PDOs with *RAS* mutations (*KRAS* mut = 14, *NRAS* mut = 3, *RAS* wt = 22; **Fig. 2A**; ref. 41), and the median DSS for cetuximab in *RAS*-mutated PDOs was 5.0 (range, 0–19), compared with 21 (range, 5.2–29) for wild-type PDOs ($P = 0.002$, Wilcoxon rank-sum test). Pharmacological associations were also found for a few targeted drugs with different mechanisms of action, such as between idasanutlin (MDM2/TP53i) and palbociclib (CDKi; Pearson's correlation 0.61) or alisertib (Aurorai; Pearson's correlation 0.51; Supplementary Fig. S5).

Most CRLMs have strong *ex vivo* vulnerabilities to selected clinical drugs

A heatmap of sensitivities to the thirty-eight evaluated drugs (drug-wise median-centered DSS values; **Fig. 2B**) showed that the PDOs formed clusters based primarily on the sensitivity to EGFR and/or MDM2 inhibition, as well as to SN-38 and nucleosides. The difference in sensitivity to MDM2 inhibition was defined by TP53 activity (**Fig. 2C**), and the four PDOs (from three patients) with the most "*TP53* wild-type–like" phenotype (based on a gene expression signature of the five most upregulated genes in *TP53* wild-type compared with mutated primary colorectal cancers) had outlier sensitivity to idasanutlin ($P = 0.0071$, Wilcoxon rank-sum test). *TP53* mutation analyses confirmed wild-type status for two of the sensitive PDOs, but identified heterozygous mutations in the two PDOs with the strongest sensitivity (both from patient 18), and additionally indicated wild-type status in a PDO with only intermediate sensitivity (*TP53* wild-type *versus* mutated: $P = 0.012$, Wilcoxon rank-sum test; **Fig. 2C**; Supplementary Fig. S6). Notably, the third PDO from patient 18 was completely resistant to MDM2 inhibition by idasanutlin.

In contrast with EGFR inhibition, sensitivity to MEK inhibition was not associated with *RAS* mutation status ($P = 0.97$ for binimetinib and $P = 1.0$ for trametinib, Wilcoxon rank sum test; **Fig. 2A**) and two *RAS*-mutated lesions from each of two patients (patient 3, *KRAS* mutated and patient 10, *NRAS* mutated) showed apparent intra-patient heterogeneity in MEK inhibitor sensitivities (patient 3: ΔDSS = 7 for trametinib and 6 for binimetinib; patient 10: ΔDSS = 9 for trametinib and 4 for binimetinib). Notably, the *RAS* wild-type PDO derived from patient 1 was resistant to both EGFR and MEK inhibitors. This PDO harbored the rare $BRAF^{D594G}$ mutation and was also resistant to the $BRAF^{V600}$ inhibitor encorafenib (**Fig. 2B**).

For approved drugs other than those targeting EGFR or MEK, we observed mostly moderate differences in drug sensitivity among the PDOs (**Fig. 2B**). The activity of 5-FU and the multi-kinase inhibitor regorafenib was generally low, although we observed fair differential drug responses below the reported maximum blood plasma concentrations (C_{max}; Supplementary Fig. S7). Encorafenib showed no activity, consistent with wild-type *BRAF* codon 600 status in all PDOs. No/limited activity was also found for oxaliplatin and TAS-102, but this was likely due to too low drug concentrations. In contrast, the active metabolite of irinotecan, SN-38, showed high activity in nearly all the PDOs with a moderate to strong differential activity. Fifteen of the twenty-two patients were treated with neoadjuvant combination therapies (5-FU, oxaliplatin, irinotecan, bevacizumab, cetuximab, and panitumumab combinations) and the PDOs showed *ex vivo* sensitivities to 5-FU, SN-38, and EGFR inhibitors corresponding with the tumor responses according to RECIST, implying recapitulation of pharmacological responses in the pre-clinical models (oxaliplatin was not compared due to low activity at the tested concentrations; Supplementary Table S3).

Strong differential drug sensitivities among the PDOs were observed for the antimetabolites methotrexate and gemcitabine (**Fig. 3A**; Supplementary Figs. S8 and S9), as well as for a number of targeted drugs that have no decisive genomic markers, but that are currently tested in late-phase clinical trials in patients with mCRC and/or other cancer types. These targeted agents included the Aurora A kinase inhibitor alisertib (phase 3), the Bcl inhibitor navitoclax (phase 2), the HSP90 inhibitor luminespib (phase 2), the dual PI3K/mTOR inhibitor gedatolisib (phase 3), and the PLK1 inhibitor volasertib (phase 3; **Fig. 3B**; Supplementary Figs. S8 and S9). There were no clear responders to crizotinib (ALK inhibitor) or LGK974 (PORCN inhibitor), likely related to the low frequency in mCRC of the genomic aberrations associated with sensitivity to these agents. In accordance, no outlier expression profiles were observed for the corresponding target genes (Supplementary Fig. S10).

Promising therapies could be nominated for eighteen (82%) of the patients based on the ranked relative DSS values and E_{max} (%

Published OnlineFirst April 16, 2020; DOI: 10.1158/1078-0432.CCR-19-3637

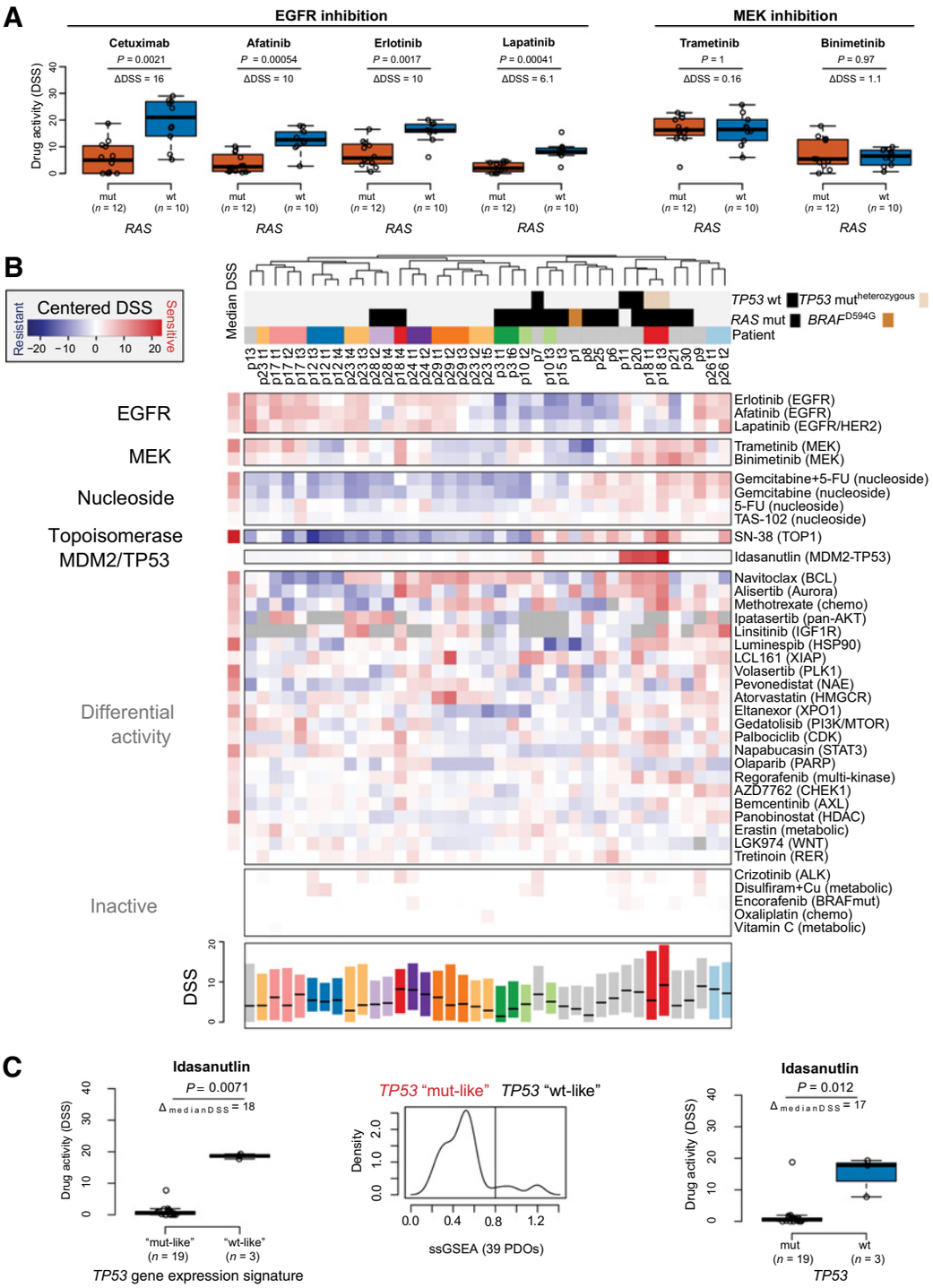

Figure 2.

Pharmacological patterns of PDOs from colorectal cancer liver metastases. **A,** Pharmacogenomic relationship between *RAS* mutation status and response to EGFR inhibition and MEK inhibition. **B,** Relative drug sensitivities across the PDO cohort. Heatmap visualizes drug-wise median-centered DSS values, with higher (red) and lower (blue) values, indicating higher and lower sensitivity, respectively. Samples were ordered by hierarchical clustering using Pearson's correlation distance and complete linkage. Drugs were manually grouped according to mechanism of action and response patterns. Missing values are indicated in gray. The boxplot below shows the distribution of DSS values per PDO, with 25th, 50th, and 75th percentiles. For pairs of highly correlated drugs, only one was included in the calculations (see Materials and Methods). **C,** Association of the *TP53* gene expression signature and *TP53* mutation status with idasanutlin sensitivity. The *P* values are from Wilcoxon rank sum tests. Δ DSS indicates difference in medians. For multi-lesion samples, the mean DSS of the lesions was used as input. Abbreviations: DSS, drug sensitivity score; p, patient; ssGSEA, single-sample gene set enrichment analysis.

Published OnlineFirst April 16, 2020; DOI: 10.1158/1078-0432.CCR-19-3637

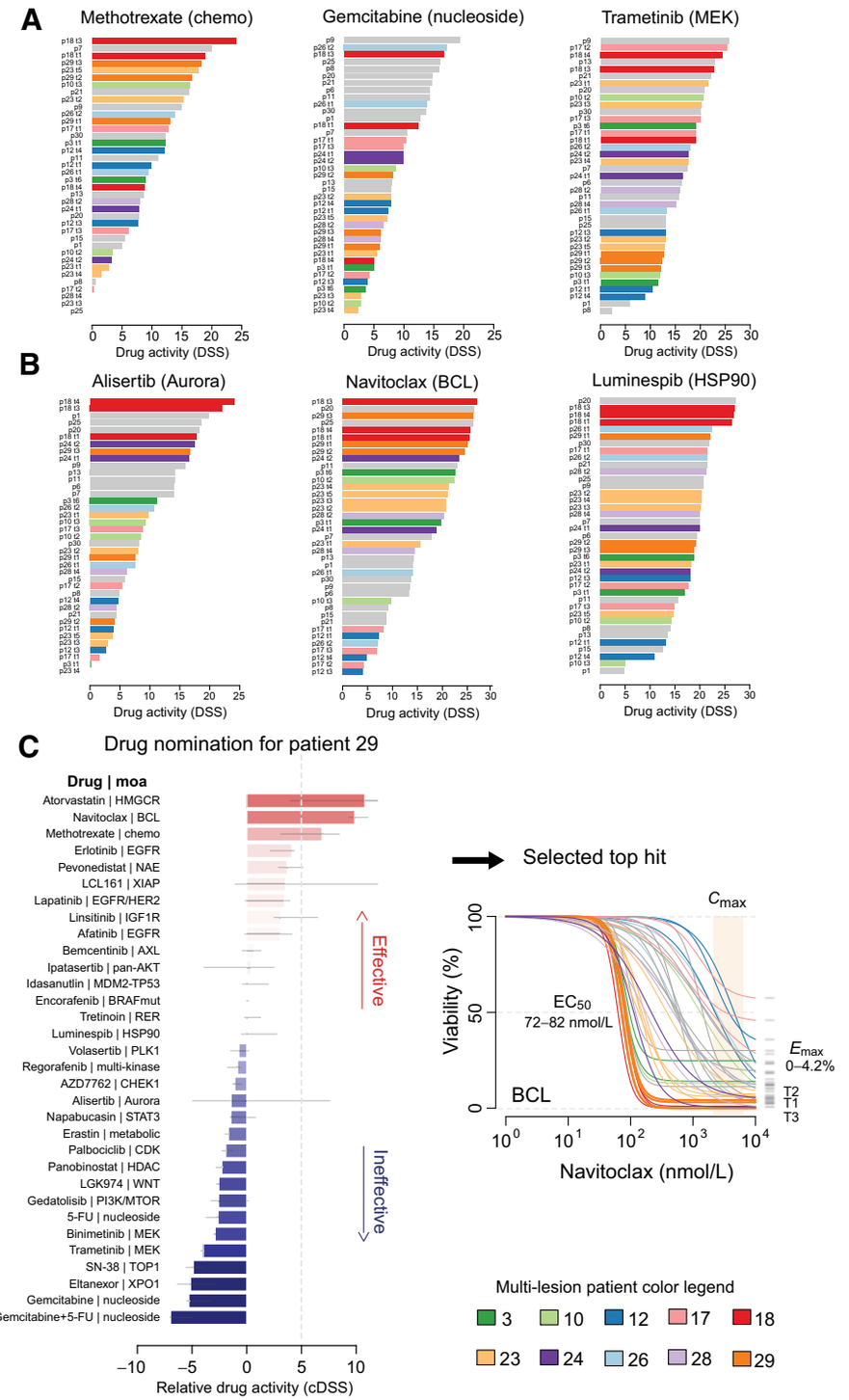

Figure 3.

Drugs with strong differential activity and personalized therapy nomination. Approved drugs (**A**) and investigational drugs (**B**) in late-phase clinical studies with strong differential activity across the PDO cohort. **C,** Illustration of use of *ex vivo* drug response profiling to nominate potential therapies for individual patients; here, patient 29. Error bars in the vertical bar plot indicate variation in median-centered DSS values between the three screened PDOs from the patient. Abbreviations: cDSS, median-centered drug sensitivity score; C_{max}, maximum plasma drug concentration; E_{max}, maximum drug activity; moa, mechanism of action; p, patient.

viability) across all drugs (**Table 1**; Supplementary Fig. S11). The PDOs from three metastatic lesions from patient 29 (**Fig. 3C**) illustrate the several heuristic parameters used for drug nominations (unambiguous dose–response curves, E_{max} < 50% viability, median-centered DSS > 5, and low DSS variation among metastases from the same patient). PDOs from seven of the patients (patients 6, 7, 9, 11, 13, 20 and 21) were generally sensitive to several drugs, including standard of care therapies (**Table 1**). PDOs derived from patients 25 and 29 were sensitive to drugs approved for other indications and drugs in phase 2/3 clinical trials, and PDOs from patients 1, 18, and 28 were sensitive only to drugs in development (in phase 2/3 trials). No drug candidates could be nominated for four (18%) of the patients (patients 3, 10, 12 and 23) according to the defined criteria. However, based on absolute (in contrast with

Published OnlineFirst April 16, 2020; DOI: 10.1158/1078-0432.CCR-19-3637

Table 1. Therapy nominations for patients based on *ex vivo* drug screen.

Patients (*multi-met)	*RAS/RAF* and *TP53* gene mutations	Standard of care	Approved therapies non-CRC	Emerging therapies selected phase 2 and 3	
p6	*KRAS*^{G13D} *TP53*^{G187splice}	SN-38/irinotecan	Atorvastatin; tretinoin	Alisertib	**Approved**
p7	*KRAS*^{G12D}	SN-38/irinotecan	Methotrexate	LCL161; idasanutlin; erastin	
p8	*KRAS*^{G12V} *TP53*^{R248W}	SN-38/irinotecan		Napabucasin; ipatasertib	
p9	*TP53*^{R248W}	Cetuximab	Gemcitabine; methotrexate; trametinib; afatinib; erlotinib	Alisertib; pevonedistat; volasertib; AZD7762; linsitinib	
p11		Cetuximab; (5-FU)	Afatinib	Idasanutlin; navitoclax; gedatolisib	
p13	*TP53*^{R213L}	Cetuximab	Lapatinib; afatinib; erlotinib;trametinib	Gedatolisib; alisertib	
p15	*KRAS*^{G13D} *TP53*^{R158L}	SN-38/irinotecan			
p17*	*TP53*^{R213*}	Cetuximab	Afatinib; erlotinib		
p20	*KRAS*^{G12D}	Regorafenib; (5-FU)	Binimetinib	Idasanutlin; navitoclax; luminespib; alisertib; LCL161	
p21	*NRAS*^{Q61A} *TP53*^{R223del}	SN-38/irinotecan; regorafenib	Binimetinib; trametinib; methotrexate; gemcitabine + 5-FU		
p24*	*TP53*^{R249W}	Cetuximab	(Erlotinib)	Alisertib	
p26*		Cetuximab	(Afatinib; erlotinib)	Linsitinib	
p30	*TP53*^{V157G}	Regorafenib	Binimetinib, atorvastatin		
p25	*KRAS*^{G13D} *TP53*^{R175H}		Gemcitabine + 5-FU	Navitoclax; alisertib; LCL161	**Off-label**
p29*	*TP53*^{W146del}		(Atorvastatin; erlotinib)	Navitoclax	
p1	*BRAF*^{D594G} *TP53*^{R273H}			Alisertib; volasertib	**Investigational**
p18*	*KRAS*^{G12V} *TP53*^{R158H}			Navitoclax; alisertib; luminespib; palbociclib	
p28*	*KRAS*^{G13D} *TP53*^{M237I}			Ipatasertib	
p3*	*KRAS*^{G12D} *TP53*^{P152del}				**None**
p10*	*NRAS*^{G12D} *TP53*^{P301ins}				
p12*	*TP53*^{N200del}	(Cetuximab)	(Afatinib; erlotinib)		
p23*	*TP53*^{R248W}				

Note: Candidates were selected among approved drugs and drugs in phase 2/3 clinical studies and showed (i) at least 50% reduction in viability, (ii) 5 DSS higher than median, and (iii) high-quality dose-response profiles. For patients with multiple lesions screened (indicated by asterisk), an additional drug selection criterion was low intra-patient inter-metastatic heterogeneity. The standard-of-care drugs SN-38 (active metabolite of irinotecan) and 5-fluorouracil (5-FU) that did not satisfy the second criterion, but nevertheless showed activity among the top 30th percentile across all patients are indicated in parentheses. Likewise, for anti-EGFR, the number of responders likely renders the median-center approach too strict and patients from which the PDOs had DSS > 10 are indicated with parentheses. Notably, patient 29 showed clear outlier sensitivity to atorvastatin, although the third PDO did not satisfy the second nomination criterion (indicated in parentheses).

relative) drug activity, the three *RAS* wild-type PDOs from patient 12 were all sensitive to EGFR inhibition (**Fig. 2B**).

There was large variation among the PDOs in the overall level of drug sensitivities and the number of strong drug vulnerabilities (**Fig. 4A**). The two PDOs from patient 26 showed an overall strong sensitivity pattern [median DSS 8.2 and 7.2; interquartile range (IQR): 13 and 14 for t1 and t2, respectively; **Fig. 4A**], whereas the PDO from patient 8 was resistant to all drugs beyond the few vulnerabilities listed in **Table 1** (median DSS 2.3; IQR: 0.3–8.9). This latter PDO also had mesenchymal-like gene expression characteristics that have been linked to drug resistance, including upregulated expression of gene sets related to "TGFβ," "EMT," "LGR5 stem cells," and "WNT," as well as downregulation of the "differentiation" and "CDX2" gene sets (**Fig. 4B**). Reduced CDX2 and CK20 protein expression further supported a poorly differentiated phenotype (**Fig. 4B**). To explore the potential for more efficient growth inhibition of this multi-drug–resistant and *KRAS*^{G12V}-mutated PDO, we designed a combination screen based on the strongest observed vulnerability: sensitivity to inhibition of the PI3K/AKT/mTOR pathway (**Fig. 4C**), which was associated with the apparent loss of *PTEN* expression (**Fig. 4D**). Combined mTOR or AKT inhibition with MEK inhibition may be synergistic in this genetic background (42, 43), and both combination screens with everolimus (mTOR) or ipatasertib (AKT) plus trametinib suggested a synergistic negative effect on PDO viability, as evaluated by a zero interaction potency model (**Fig. 4E**).

Intra-patient inter-metastatic pharmacotranscriptomic heterogeneity is not pronounced

Comparisons of the pharmacological profiles of PDOs from multiple CRLMs from each of ten patients showed strong intra-patient

Published OnlineFirst April 16, 2020; DOI: 10.1158/1078-0432.CCR-19-3637

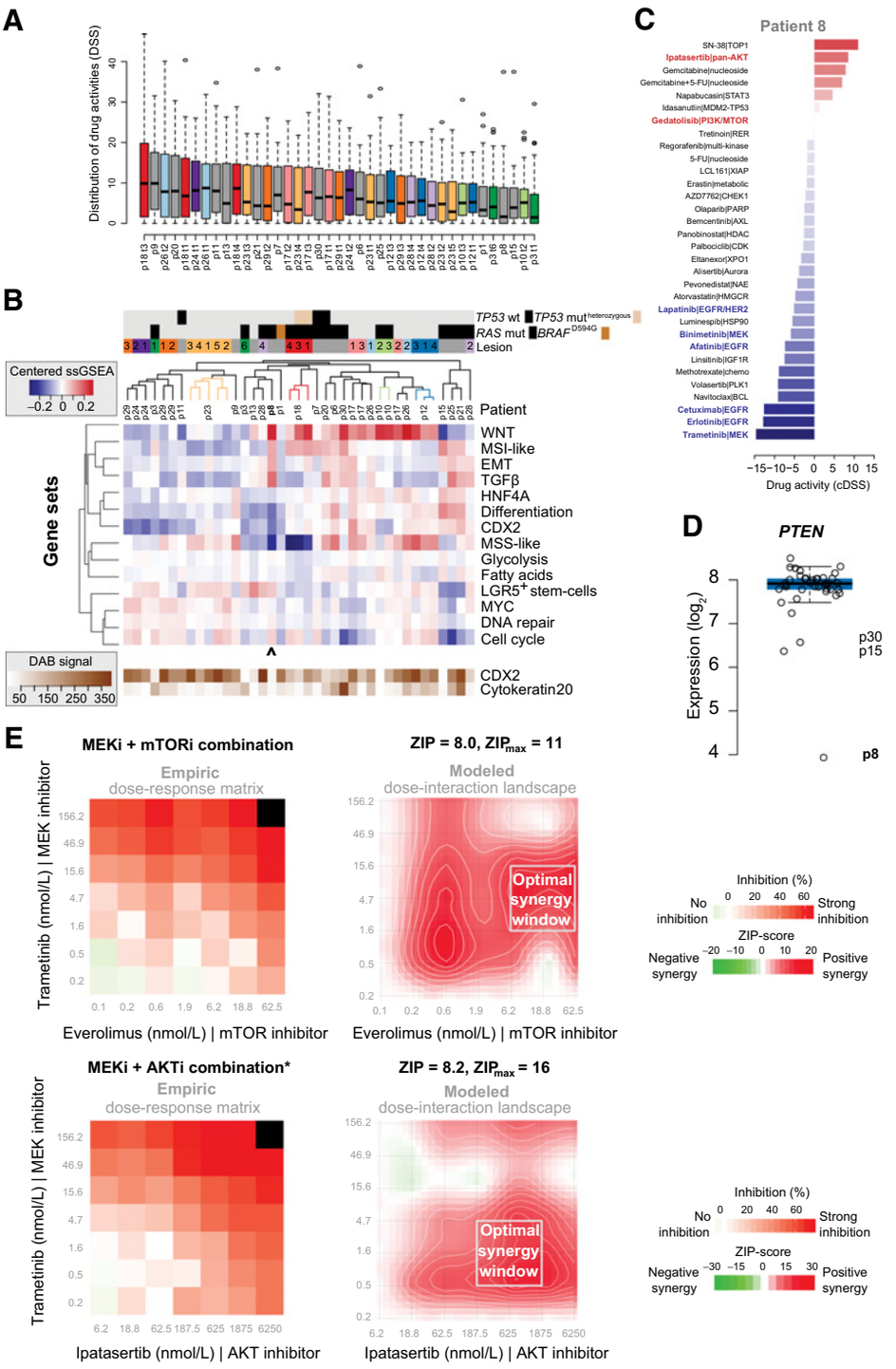

Figure 4.

Pharmacogenomic relationships for PDOs. **A,** Distribution of drug activities in PDOs ranked by 75th percentile. **B,** Gene set enrichment analysis of PDOs showing median-centered scores for fourteen pre-specified gene sets (see Materials and Methods). Samples and gene sets were clustered according to correlation distance and average linkage. Protein expressions for CDX2 (caudal type homeobox 2 transcription factor) and CK20 (cytokeratin 20) are shown below. **C,** Waterfall plot of median-centered DSS for patient 8. Higher values indicate higher activity relative to other PDOs. The four drugs with cross-dataset range in DSS <5 were excluded. **D,** *PTEN* expression in PDOs, showing particularly low expression levels for patients 8, 15, and 30. **E,** Drug synergy testing between MEK inhibition and mTOR or AKT inhibition in PDO with *PTEN* loss. cDSS, median-centered drug sensitivity score; DAB, 3,3′-diaminobenzidine; p, patient; ssGSEA, single-sample gene set enrichment analysis; ZIP, zero interaction potency. *The ipatasertib plus trametinib combination was performed in replicate due to the overall technical variability observed for ipatasertib (Supplementary Fig. S4C), showing comparable results (ZIP = 5, ZIP_{max} = 10).

correspondences in drug sensitivities to the majority of the tested drugs. The multiple PDOs largely clustered patient-wise, both in hierarchical clustering and PCA (**Figs. 2B** and **5A**). By careful evaluation of all dose–response curves we observed convincing inter-metastatic heterogeneity (not associated with technical variability in replicate screens) in less than one tenth of all the 38 × 10 drug–patient comparisons, including in patient 3 (MEKi), patient 10 (MEKi and navitoclax), patient 18 (idasanutlin), patient 23 (EGFRi/MEKi) and patient 29 (LCL 161). The differential response to idasanutlin in patient 18 was associated with heterozygous *versus* homozygous *TP53* mutation status in the sensitive *versus* resistant PDOs, but all PDOs from this patient had a TP53 wild-type–like phenotype by gene expression. Furthermore, although a gene expression signature of sensitivity to EGFR inhibition (23) was correlated with erlotinib

Published OnlineFirst April 16, 2020; DOI: 10.1158/1078-0432.CCR-19-3637

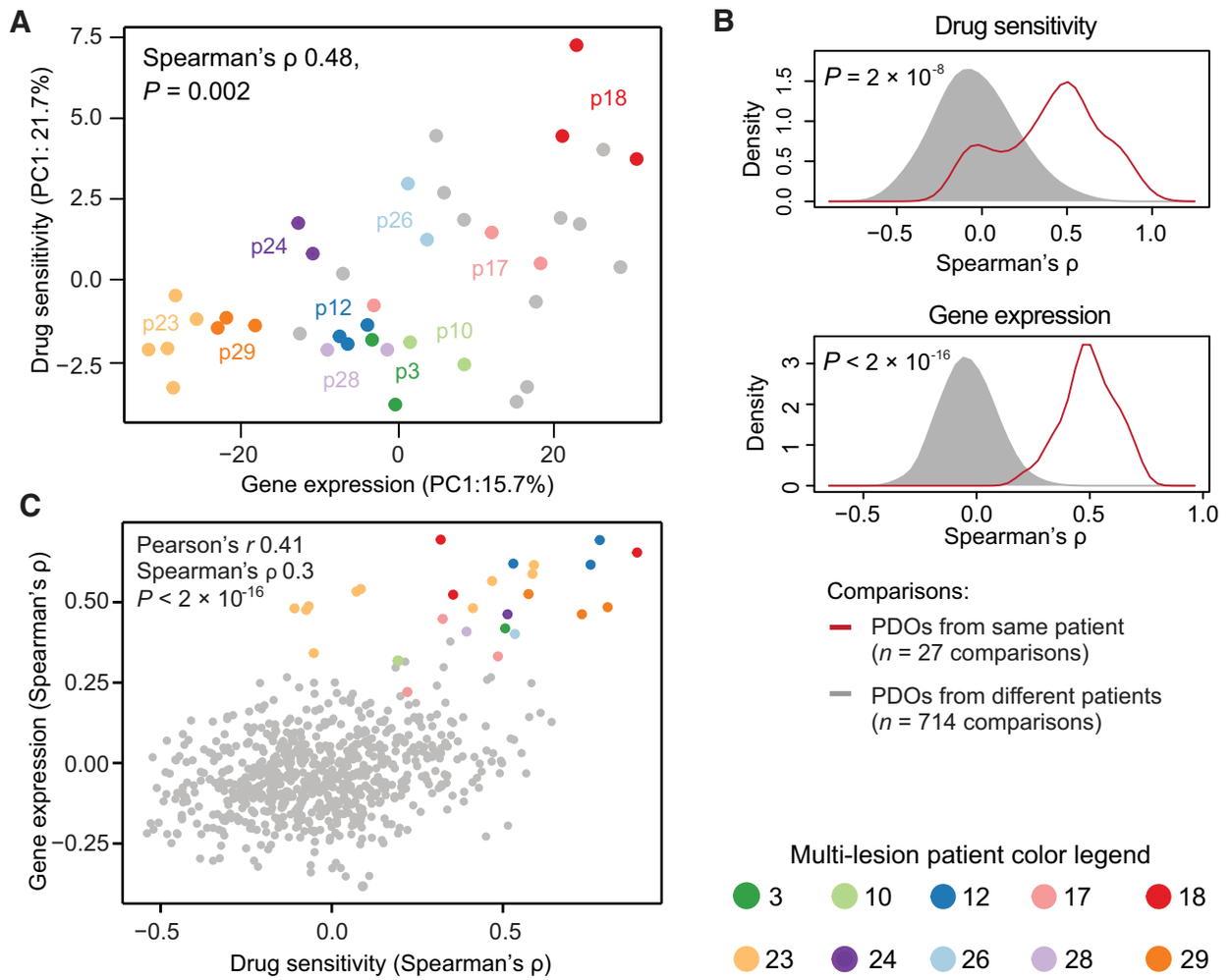

Figure 5.

Correspondence between drug sensitivity and gene expression variation. **A,** Principal component analyses of drug sensitivity (*y*-axis) and gene expression profiles (*x*-axis) of PDOs. PDOs derived from multiple CRLMs from each of ten patients are color coded and indicated with patient numbers. All other PDOs are shown in gray. Two drugs with frequent NAs (linsitinib and ipatasertib), and the seven drugs with lowest cross-sample variance (vitamin C, oxaliplatin, encorafenib, disulfiram, crizotinib, TAS-102, and tretinoin) were excluded from PCA analyses of drug sensitivity. **B,** Distributions of Spearman's correlation coefficients for drug sensitivity and gene expression separately. Correlations for related and unrelated PDOs are indicated. **C,** Scatterplot of Spearman's correlation coefficients between pairs of PDOs at the drug sensitivity (horizontal axis) and gene expression (vertical axis) levels. Linsitinib and ipatasertib were excluded also from analyses in (**B**) and (**C**) due to frequent NAs. Each dot represents one comparison between two PDOs, and comparisons of PDOs from the same patient are color coded, whereas comparisons of unrelated PDOs are shown in gray. Note: the PCA function does missing value imputation (by mean of variable). Abbreviations: p, patient; PC, principal component.

sensitivity across all PDOs, this could not explain the inter-metastatic pharmacological heterogeneity to EGFRi/MEKi among five *RAS*/*BRAF* wild-type PDOs from patient 23 (Supplementary Fig. S12).

Gene expression profiles were similarly compared to investigate the extent to which the variation in drug sensitivities was recapitulated at the mRNA level. Gene set analyses in PDOs confirmed that PDOs from the same patients clustered more closely in hierarchical clustering analyses than unrelated PDOs also at the gene expression level (**Fig. 4B**). Furthermore, PCA comparisons showed a significant correlation of PC1 values at the gene expression and drug sensitivity levels (Spearman's ρ 0.48, $P = 0.002$), largely with sample-wise clustering of PDOs in both dimensions (**Fig. 5A**). Intra-patient correspondence was further confirmed by comparisons of pairwise Spearman's correlation coefficients for either drug sensitivity or gene expression between different tumors from the same patient and between tumors from different patients (**Fig. 5B**). PDOs from the same patients had stronger correlations at both levels, indicating lower intra-patient compared with inter-patient heterogeneity. Pairwise comparisons of Spearman's correlation coefficients for DSS and gene expression between PDOs demonstrated that both unrelated and related PDOs were correlated at the two different data levels, although PDOs from different lesions from the same patient had the strongest correlation (**Fig. 5C**).

Discussion

In this study, we have established a platform for *ex vivo* pharmacogenomic profiling of metastatic tumors from patients with colorectal

Published OnlineFirst April 16, 2020; DOI: 10.1158/1078-0432.CCR-19-3637

cancer, acknowledging the strong association between metastasis and cancer-associated mortality (44), as well as the potential difference in biology and target modulation between primary and metastatic tumors. Patients with mCRC have relatively few treatment options, and development of resistance to systemic therapies almost invariably occurs (8). We show marked variation among patients in sensitivity to several anticancer agents not currently approved for colorectal cancer, and identified patients with strong differential sensitivity to both chemotherapies and targeted agents. Antimetabolites (gemcitabine and methotrexate) and several targeted agents with no clear genomic marker, such as the mitotic inhibitor alisertib and the apoptosis inducer navitoclax, showed stronger inter-patient heterogeneity of anticancer activities than most of the approved chemotherapies. This underscores the opportunity for successful off-label drug prescription in colorectal cancer, although it should be noted that the moderate differential activities observed for commonly used chemotherapies may reflect prior treatments given to the patients included in this observational study.

Clustering analyses of the drug sensitivity data demonstrated three main response groups among the PDOs, defined by sensitivity to EGFR and/or MDM2 inhibition, or resistance to both. Although likely influenced by the inclusion of several agents targeting EGFR in the drug testing panel, this separation was also reflected on the genomic and transcriptomic levels, specifically by the well-known markers *RAS* mutation and TP53 activity. Notably, the "double-resistant" subgroup with *RAS* and *TP53* co-mutations has known poor prognostic associations after hepatic resection (45, 46), reinforcing the challenge of adequate management of these patients. On the basis of pre-defined, although not yet clinically validated drug nomination criteria, we could suggest potentially effective therapies for eighteen of the twenty-two patients, including seven of the nine patients with *RAS* and *TP53* co-mutations. Prospective validation in co-clinical trials is necessary to evaluate the clinical utility of this drug nomination strategy. We are continuing prospective patient inclusion in the observational study, and are currently planning an interventional study for clinical translation of our *ex vivo* pharmacogenomics platform for patients with relapse after hepatic resection and/or non-resectable CRLM. A step forward was taken last fall, when Ooft and colleagues (47) showed that *ex vivo* drug screen of PDOs correctly predicted response of irinotecan-based chemotherapy in patients with mCRC.

By inclusion of multiple distinct metastatic lesions from each of ten patients, we show that intra-patient inter-metastatic pharmacological heterogeneity is not pronounced for the thirty-eight evaluable drugs in this study. The consistent intra-patient response pattern for the majority of drugs is highly encouraging with respect to development of novel therapies for patients with mCRC. Intra-patient inter-metastatic heterogeneity in clinical responses to both molecularly targeted agents (16, 48) and chemotherapies (14, 15) have been reported in mCRC, the latter in subgroups of approximately 10% to 25% of patients (14, 15). Furthermore, acquired resistance during treatment is a major challenge for treatment efficacy (13, 49), highlighting the relevance of longitudinal pharmacogenomic profiling. Demonstration of pharmacological diversification on the single-cell level (29) also suggests potential development of independent resistance mechanisms in different metastatic lesions from individual patients. In our study, clear instances of intra-patient heterogeneous responses were relatively uncommon with less than one tenth of all drug/patient pairs showing convincing inter-metastatic variation, even less if the similar mechanism of action of several of the drugs was taken into account. It should be noted that our study neither provided single-cell resolution nor evaluated pharmacological profiles in extra-hepatic tumors for patients with widespread dissemination, and this may impact the estimates of intra-patient pharmacological heterogeneity.

With the exception of *RAS* mutations and TP53 activity, there was an evident lack of molecular markers for most of the drugs with differential activity among patients in this study. This is associated with the low prevalence of most known drug targets in mCRC, including $BRAF^{V600E}$ mutations and kinase gene fusions (50), for which the matched drugs showed no activity in any of the PDOs. Although the number of samples was insufficient to develop robust molecular prediction signatures in this initial phase of the project, "pharmaco-transcriptomic" integration analyses showed that gene expression profiles recapitulated much of the variation in pharmacological profiles. This "co-variation" in pharmacological and transcriptomic profiles is in accordance with an anticipated close relationship between cell phenotypes and drug responses (51), but has to our knowledge not been previously characterized in the intra-patient inter-metastatic setting. This suggests that drug response prediction could be improved by incorporating transcriptomic profiling in addition to genomic predictive markers, a strategy that was recently assessed in the WINTHER trial (52). Furthermore, gene expression characteristics of a mesenchymal phenotype, which has repeatedly been linked to drug resistance (53, 54), were found in a *RAS*-mutated multi-drug resistant PDO with loss of *PTEN* expression. Increased sensitivity to combined treatment with trametinib and ipatasertib or everolimus in this PDO also suggests that *ex vivo* pharmacotranscriptomic profiling might prove useful to guide the development of targeted combination therapies.

We detected a rare class 3 $BRAF^{D594G}$ mutation in both the CRLM and PDO from patient 1. This mutation leads to RAS-dependent kinase inactivation and has been reported to associate with a different histopathology and a markedly longer overall patient survival than class 1 $BRAF^{V600E}$ mutations (55). The mutation is not a target for approved BRAF inhibitors, and accordingly the PDO did not show any response to encorafenib. Available data with respect to prediction of sensitivity to EGFR inhibition with this mutation class are inconclusive, but the PDO was resistant to both EGFR and MEK inhibition despite wild-type *RAS* status, highlighting the current lack of an optimal strategy to target cancers with this mutation. The PDO had a median overall level of drug sensitivities compared with other PDOs included in this study, and the strongest robust response was to the oral inhibitor alisertib, targeting the mitotic regulator Aurora A kinase.

The PDOs differed noticeably in their growth rate, but the median time from surgery to completed drug screen was two months, indicating that pharmacological profiling of PDOs can be performed within a clinically relevant timeframe for patients with resected CRLM, for which the relapse rate is approximately 70% to 80% (56). We also showed that the functional screen was robust by demonstrating high reproducibility of replicate and repeated screens, strong correlation between drugs of a similar functional class, and recapitulation of known pharmacogenomic associations. We are planning a study for clinical translation of this pharmacogenomic platform and to investigate its potential to guide experimental therapies for patients with mCRC.

Disclosure of Potential Conflicts of Interest

H.G. Palmer reports receiving commercial research grants from Novartis, Blueprint, Bayer, and Merus. R. Dienstmann is an employee/paid consultant for Roche, Boehringer Ingelheim, and reports receiving speakers bureau honoraria from Roche, Servier, Ipsen, Amgen, Sanofi, and Merck Sharp Dohme. No potential conflicts of interest were disclosed by the other authors.

Published OnlineFirst April 16, 2020; DOI: 10.1158/1078-0432.CCR-19-3637

Authors' Contributions

Conception and design: J. Bruun, K. Kryeziu, P.W. Eide, B. Røsok, R. Dienstmann, A. Nesbakken, B.A. Bjørnbeth, A. Sveen, R.A. Lothe
Development of methodology: J. Bruun, K. Kryeziu, P.W. Eide, R.A. Lothe
Acquisition of data (provided animals, acquired and managed patients, provided facilities, etc.): J. Bruun, K. Kryeziu, S.H. Moosavi, I.A. Eilertsen, J. Langerud, B. Røsok, M.Z. Totland, T.H. Brunsell, T. Pellinen, J. Saarela, C.H. Bergsland, H.G. Palmer, K.W. Brudvik, M.G. Guren, A. Nesbakken, B.A. Bjørnbeth, A. Sveen, R.A. Lothe
Analysis and interpretation of data (e.g., statistical analysis, biostatistics, computational analysis): J. Bruun, K. Kryeziu, P.W. Eide, S.H. Moosavi, T.H. Brunsell, K.W. Brudvik, T. Guren, R. Dienstmann, M.G. Guren, A. Nesbakken, B.A. Bjørnbeth, A. Sveen, R.A. Lothe
Writing, review, and/or revision of the manuscript: J. Bruun, K. Kryeziu, P.W. Eide, I.A. Eilertsen, J. Langerud, B. Røsok, M.Z. Totland, T.H. Brunsell, T. Pellinen, J. Saarela, C.H. Bergsland, K.W. Brudvik, T. Guren, R. Dienstmann, M.G. Guren, A. Nesbakken, B.A. Bjørnbeth, A. Sveen, R.A. Lothe
Administrative, technical, or material support (i.e., reporting or organizing data, constructing databases): J. Bruun, K. Kryeziu, K.W. Brudvik, A. Nesbakken, B.A. Bjørnbeth, R.A. Lothe, P.W. Eide, A. Sveen
Study supervision: R.A. Lothe

Acknowledgments

We acknowledge the technical support from Merete Bjørnslett, Merete Hektoen and Mette Eknæs, Department of Molecular Oncology, Oslo University Hospital (OUH) and from the project study nurses Vlora Krasniqi Hula and Magdalena Kowalewska-Harbiyeli at the Department of Hepato-Pancreato-Biliary Surgery, OUH, all members of the K.G. Jebsen Colorectal Cancer Research Center. We appreciate the help from the technical team at the High Throughput Biomedicine Unit (HTB) at the Institute for Molecular Medicine Finland (FIMM), with a special thanks to Laura Turunen for advice on the design of the drug library. The FIMM High Throughput Biomedicine Unit is financially supported by the University of Helsinki and Biocenter Finland. We are grateful to the laboratories of Prof. Hans Clevers (Hubrecht Institute), Prof. Toshiro Sato (Keiko University), Prof. Emile Voest (Netherlands Cancer Institute), Prof. Calvin Kuo (Stanford University), and Dr. Bon-Kyoung Koo (Cambridge Stem Cell Institute) for sharing tips and laboratory protocols for organoid cell culture. The study was financially supported by the Norwegian Cancer Society [project numbers 6824048-2016 (to A. Sveen) and 182759-2016 (to R.A. Lothe supporting K. Kryeziu as staff scientist)], the foundation "Stiftelsen Kristian Gerhard Jebsen" (supports I.A. Eilertsen, S.H. Moosavi, and T.H. Brunsell as PhD students), the South-Eastern Norway Regional Health Authority [project numbers 2016123 (to R.A. Lothe supporting C.H. Bergsland as PhD student) and 2017102 (to R.A. Lothe supporting P.W. Eide as post doc], and the Research Council of Norway [FRIPRO Toppforsk, project number 250993 (to R.A. Lothe supporting J. Langerud as PhD student)].

The costs of publication of this article were defrayed in part by the payment of page charges. This article must therefore be hereby marked *advertisement* in accordance with 18 U.S.C. Section 1734 solely to indicate this fact.

Received November 5, 2019; revised March 2, 2020; accepted April 10, 2020; published first April 16, 2020.

References

1. Bray F, Ferlay J, Soerjomataram I, Siegel RL, Torre LA, Jemal A. Global cancer statistics 2018: GLOBOCAN estimates of incidence and mortality worldwide for 36 cancers in 185 countries. CA Cancer J Clin 2018;68:394–424.
2. Helling TS, Martin M. Cause of death from liver metastases in colorectal cancer. Ann Surg Oncol 2014;21:501–6.
3. Van Cutsem E, Cervantes A, Adam R, Sobrero A, Van Krieken JH, Aderka D, et al. ESMO consensus guidelines for the management of patients with metastatic colorectal cancer. Ann Oncol 2016;27:1386–422.
4. Tabernero J, Yoshino T, Cohn AL, Obermannova R, Bodoky G, Garcia-Carbonero R, et al. Ramucirumab versus placebo in combination with second-line FOLFIRI in patients with metastatic colorectal carcinoma that progressed during or after first-line therapy with bevacizumab, oxaliplatin, and a fluoropyrimidine (RAISE): a randomised, double-blind, multicentre, phase 3 study. Lancet Oncol 2015;16:499–508.
5. Grothey A, Van Cutsem E, Sobrero A, Siena S, Falcone A, Ychou M, et al. Regorafenib monotherapy for previously treated metastatic colorectal cancer (CORRECT): an international, multicentre, randomised, placebo-controlled, phase 3 trial. Lancet 2013;381:303–12.
6. Cremolini C, Schirripa M, Antoniotti C, Moretto R, Salvatore L, Masi G, et al. First-line chemotherapy for mCRC-a review and evidence-based algorithm. Nat Rev Clin Oncol 2015;12:607–19.
7. Hammond WA, Swaika A, Mody K. Pharmacologic resistance in colorectal cancer: a review. Ther Adv Med Oncol 2016;8:57–84.
8. Dienstmann R, Vermeulen L, Guinney J, Kopetz S, Tejpar S, Tabernero J. Consensus molecular subtypes and the evolution of precision medicine in colorectal cancer. Nat Rev Cancer 2017;17:79–92.
9. Overman MJ, Lonardi S, Wong KYM, Lenz HJ, Gelsomino F, Aglietta M, et al. Durable clinical benefit with nivolumab plus ipilimumab in DNA mismatch repair-deficient/microsatellite instability-high metastatic colorectal cancer. J Clin Oncol 2018;36:773–9.
10. Kopetz S, Grothey A, Yaeger R, Van Cutsem E, Desai J, Yoshino T, et al. Encorafenib, binimetinib, and cetuximab in BRAF V600E-mutated colorectal cancer. N Engl J Med 2019;381:1632–43.
11. Sartore-Bianchi A, Trusolino L, Martino C, Bencardino K, Lonardi S, Bergamo F, et al. Dual-targeted therapy with trastuzumab and lapatinib in treatment-refractory, KRAS codon 12/13 wild-type, HER2-positive metastatic colorectal cancer (HERACLES): a proof-of-concept, multicentre, open-label, phase 2 trial. Lancet Oncol 2016;17:738–46.
12. Sveen A, Loes IM, Alagaratnam S, Nilsen G, Holand M, Lingjaerde OC, et al. Intra-patient inter-metastatic genetic heterogeneity in colorectal cancer as a key determinant of survival after curative liver resection. PLoS Genet 2016;12:e1006225.
13. Misale S, Yaeger R, Hobor S, Scala E, Janakiraman M, Liska D, et al. Emergence of KRAS mutations and acquired resistance to anti-EGFR therapy in colorectal cancer. Nature 2012;486:532–6.
14. van Kessel CS, Samim M, Koopman M, van den Bosch MA, Borel Rinkes IH, Punt CJ, et al. Radiological heterogeneity in response to chemotherapy is associated with poor survival in patients with colorectal liver metastases. Eur J Cancer 2013;49:2486–93.
15. Brunsell TH, Cengija V, Sveen A, Bjornbeth BA, Rosok BI, Brudvik KW, et al. Heterogeneous radiological response to neoadjuvant therapy is associated with poor prognosis after resection of colorectal liver metastases. Eur J Surg Oncol 2019;45:2340–6.
16. Siravegna G, Lazzari L, Crisafulli G, Sartore-Bianchi A, Mussolin B, Cassingena A, et al. Radiologic and genomic evolution of individual metastases during HER2 blockade in colorectal cancer. Cancer Cell 2018;34:148–62.
17. Russo M, Siravegna G, Blaszkowsky LS, Corti G, Crisafulli G, Ahronian LG, et al. Tumor heterogeneity and lesion-specific response to targeted therapy in colorectal cancer. Cancer Discov 2016;6:147–53.
18. Marquart J, Chen EY, Prasad V. Estimation of the percentage of US patients with cancer who benefit from genome-driven oncology. JAMA Oncol 2018;4:1093–8.
19. Dienstmann R, Tabernero J. Cancer: a precision approach to tumour treatment. Nature 2017;548:40–1.
20. van de Wetering M, Francies HE, Francis JM, Bounova G, Iorio F, Pronk A, et al. Prospective derivation of a living organoid biobank of colorectal cancer patients. Cell 2015;161:933–45.
21. Weeber F, van de Wetering M, Hoogstraat M, Dijkstra KK, Krijgsman O, Kuilman T, et al. Preserved genetic diversity in organoids cultured from biopsies of human colorectal cancer metastases. Proc Natl Acad Sci U S A 2015;112:13308–11.
22. Fujii M, Shimokawa M, Date S, Takano A, Matano M, Nanki K, et al. A colorectal tumor organoid library demonstrates progressive loss of niche factor requirements during tumorigenesis. Cell Stem Cell 2016;18:827–38.
23. Schutte M, Risch T, Abdavi-Azar N, Boehnke K, Schumacher D, Keil M, et al. Molecular dissection of colorectal cancer in pre-clinical models identifies biomarkers predicting sensitivity to EGFR inhibitors. Nat Commun 2017;8:14262.
24. Pauli C, Hopkins BD, Prandi D, Shaw R, Fedrizzi T, Sboner A, et al. Personalized *in vitro* and *in vivo* cancer models to guide precision medicine. Cancer Discov 2017;7:462–77.

Published OnlineFirst April 16, 2020; DOI: 10.1158/1078-0432.CCR-19-3637

25. Vlachogiannis G, Hedayat S, Vatsiou A, Jamin Y, Fernandez-Mateos J, Khan K, et al. Patient-derived organoids model treatment response of metastatic gastrointestinal cancers. Science 2018;359:920–6.
26. Tiriac H, Belleau P, Engle DD, Plenker D, Deschenes A, Somerville TDD, et al. Organoid profiling identifies common responders to chemotherapy in pancreatic cancer. Cancer Discov 2018;8:1112–29.
27. Yao Y, Xu X, Yang L, Zhu J, Wan J, Shen L, et al. Patient-derived organoids predict chemoradiation responses of locally advanced rectal cancer. Cell Stem Cell 2020;26:17–26.
28. Pasch CA, Favreau PF, Yueh AE, Babiarz CP, Gillette A, Sharick JT, et al. Patient-derived cancer organoid cultures to predict sensitivity to chemotherapy and radiation. Clin Cancer Res 2019;25:5376–87.
29. Roerink SF, Sasaki N, Lee-Six H, Young MD, Alexandrov LB, Behjati S, et al. Intra-tumour diversification in colorectal cancer at the single-cell level. Nature 2018;556:457–62.
30. Schumacher D, Andrieux G, Boehnke K, Keil M, Silvestri A, Silvestrov M, et al. Heterogeneous pathway activation and drug response modelled in colorectal-tumor-derived 3D cultures. PLoS Genet 2019;15:e1008076.
31. Fujii M, Matano M, Nanki K, Sato T. Efficient genetic engineering of human intestinal organoids using electroporation. Nat Protoc 2015;10:1474–85.
32. Sveen A, Bruun J, Eide PW, Eilertsen IA, Ramirez L, Murumägi A, et al. Colorectal cancer consensus molecular subtypes translated to preclinical models uncover potentially targetable cancer cell dependencies. Clin Cancer Res 2018;24:794–806.
33. Smirnov P, Safikhani Z, El-Hachem N, Wang D, She A, Olsen C, et al. PharmacoGx: an R package for analysis of large pharmacogenomic datasets. Bioinformatics 2016;32:1244–6.
34. Yadav B, Pemovska T, Szwajda A, Kulesskiy E, Kontro M, Karjalainen R, et al. Quantitative scoring of differential drug sensitivity for individually optimized anticancer therapies. Sci Rep 2014;4:5193.
35. Yadav B, Wennerberg K, Aittokallio T, Tang J. Searching for drug synergy in complex dose-response landscapes using an interaction potency model. Comput Struct Biotechnol J 2015;13:504–13.
36. Johnson WE, Li C, Rabinovic A. Adjusting batch effects in microarray expression data using empirical Bayes methods. Biostatistics 2007;8:118–27.
37. Leek JT, Johnson WE, Parker HS, Jaffe AE, Storey JD. The sva package for removing batch effects and other unwanted variation in high-throughput experiments. Bioinformatics 2012;28:882–3.
38. Kuhn A. Correspondence regarding Zhong et al., BMC Bioinformatics 2013 Mar 7;14:89. BMC Bioinformatics 2014;15:347.
39. Eide PW, Bruun J, Lothe RA, Sveen A. CMScaller: an R package for consensus molecular subtyping of colorectal cancer pre-clinical models. Sci Rep 2017;7:16618.
40. Wagner S, Vlachogiannis G, De Haven Brandon A, Valenti M, Box G, Jenkins L, et al. Suppression of interferon gene expression overcomes resistance to MEK inhibition in KRAS-mutant colorectal cancer. Oncogene 2019;38:1717–33.
41. De Roock W, Claes B, Bernasconi D, De Schutter J, Biesmans B, Fountzilas G, et al. Effects of KRAS, BRAF, NRAS, and PIK3CA mutations on the efficacy of cetuximab plus chemotherapy in chemotherapy-refractory metastatic colorectal cancer: a retrospective consortium analysis. Lancet Oncol 2010;11:753–62.
42. Milella M, Falcone I, Conciatori F, Matteoni S, Sacconi A, De Luca T, et al. PTEN status is a crucial determinant of the functional outcome of combined MEK and mTOR inhibition in cancer. Sci Rep 2017;7:43013.
43. Weisner J, Landel I, Reintjes C, Uhlenbrock N, Trajkovic-Arsic M, Dienstbier N, et al. Preclinical efficacy of covalent-allosteric AKT inhibitor borussertib in combination with trametinib in KRAS-mutant pancreatic and colorectal cancer. Cancer Res 2019;79:2367–78.
44. Chaffer CL, Weinberg RA. A perspective on cancer cell metastasis. Science 2011;331:1559–64.
45. Chun YS, Passot G, Yamashita S, Nusrat M, Katsonis P, Loree JM, et al. Deleterious effect of RAS and evolutionary high-risk TP53 double mutation in colorectal liver metastases. Ann Surg 2019;269:917–23.
46. Kawaguchi Y, Lillemoe HA, Panettieri E, Chun YS, Tzeng CD, Aloia TA, et al. Conditional recurrence-free survival after resection of colorectal liver metastases: persistent deleterious association with RAS and TP53 co-mutation. J Am Coll Surg 2019;229:286–94.
47. Ooft SN, Weeber F, Dijkstra KK, McLean CM, Kaing S, van Werkhoven E, et al. Patient-derived organoids can predict response to chemotherapy in metastatic colorectal cancer patients. Sci Transl Med 2019;11:pii: eaay2574.
48. Germano G, Mauri G, Siravegna G, Dive C, Pierce J, Di Nicolantonio F, et al. Parallel evaluation of circulating tumor DNA and circulating tumor cells in metastatic colorectal cancer. Clin Colorectal Cancer 2018;17:80–3.
49. Siravegna G, Mussolin B, Buscarino M, Corti G, Cassingena A, Crisafulli G, et al. Clonal evolution and resistance to EGFR blockade in the blood of colorectal cancer patients. Nat Med 2015;21:795–801.
50. Sveen A, Kopetz S, Lothe RA. Biomarker-guided therapy for colorectal cancer: strength in complexity. Nat Rev Clin Oncol 2020;17:11–32.
51. Iorio F, Knijnenburg TA, Vis DJ, Bignell GR, Menden MP, Schubert M, et al. A landscape of pharmacogenomic interactions in cancer. Cell 2016;166:740–54.
52. Rodon J, Soria JC, Berger R, Miller WH, Rubin E, Kugel A, et al. Genomic and transcriptomic profiling expands precision cancer medicine: the WINTHER trial. Nat Med 2019;25:751–8.
53. Isella C, Terrasi A, Bellomo SE, Petti C, Galatola G, Muratore A, et al. Stromal contribution to the colorectal cancer transcriptome. Nat Genet 2015;47:312–9.
54. Calon A, Lonardo E, Berenguer-Llergo A, Espinet E, Hernando-Momblona X, Iglesias M, et al. Stromal gene expression defines poor-prognosis subtypes in colorectal cancer. Nat Genet 2015;47:320–9.
55. Schirripa M, Biason P, Lonardi S, Pella N, Pino MS, Urbano F, et al. Class 1, 2, and 3 BRAF-mutated metastatic colorectal cancer: a detailed clinical, pathologic, and molecular characterization. Clin Cancer Res 2019;25:3954–61.
56. Sorbye H. Recurrence patterns after resection of liver metastases from colorectal cancer. Recent Results Cancer Res 2014;203:243–52.

AACR American Association for Cancer Research

Clinical Cancer Research

Patient-Derived Organoids from Multiple Colorectal Cancer Liver Metastases Reveal Moderate Intra-patient Pharmacotranscriptomic Heterogeneity

Jarle Bruun, Kushtrim Kryeziu, Peter W. Eide, et al.

Clin Cancer Res 2020;26:4107-4119. Published OnlineFirst April 16, 2020.